# In situ disposal of crushed concrete waste as void fill material at UK nuclear sites: Leaching behavior and effect of pH on trace element release

Danielle C. Tompkins [a], Douglas I. Stewart [b], James T. Graham [c], Ian T. Burke [a,*]

[a] *School of Earth and Environment, University of Leeds, Leeds LS2 9JT, UK*
[b] *School of Civil Engineering, University of Leeds, Leeds LS2 9JT, UK*
[c] *National Nuclear Laboratory Ltd., Sellafield CA20 1PG, UK*

## ARTICLE INFO

## ABSTRACT

The leaching behavior of stockpiled crushed concrete waste is important in determining its suitability for in situ disposal at UK nuclear sites. Sand sized particles from surface (0–0.1 m) and subsurface (2.5–2.7 m) samples were composed of silica and calcite grains in a matrix of calcium alumina-silicate hydrate (C-(A)-S-H) with Ca/Si ratios of 0.5 $\pm$0.3 and 0.9 $\pm$0.3 respectively. Calcite content was also higher in surface samples indicating a greater degree of weathering and carbonation. This resulted in lower leachate pH for the surface samples (pH 8–9.6) compared to subsurface samples (pH 10–11.3). The waste displayed a high acid buffering capacity but low alkaline buffering capacity. Element release as a function of pH was similar for surface and sub-surface samples and between different size fractions. Leaching of contaminant metals was close to minimum values at the pH values produced by the crushed concrete but increased by several orders of magnitude at pH <5 (for Al, Pb, Cr and V) and pH >12 (for Al and Pb). Weathering and carbonation during long-term stockpiling, therefore, has a positive impact by producing a waste with stable pH and low metal leaching potential suitable for in-situ disposal as a void fill material.

## 1. Introduction

Concrete will form a significant proportion of the waste generated during the decommissioning and clean-up of nuclear sites across the world (IAEA, 2008, GRR, 2018). Decommissioning of 10 Magnox reactors in the UK is estimated to produce 1.3 Mt of concrete demolition waste over several decades. (NDA, 2020). Waste management options for non-contaminated and contaminated structural wastes include disposal to landfill or to a dedicated radioactive waste repository (Deissmann et al., 2006). Off-site disposal is least favored pathway in the UK's Waste Management Hierarchy (NDA, 2010) and transport of contaminated materials may pose a risk to public health if not managed correctly (Jefferson, 2009). The majority of this waste will be non-radioactive and resembles conventional demolition materials. Therefore, leaving existing below ground structures in-situ and using concrete demolition materials to backfill voids is currently under consideration (Deissmann et al., 2006; IAEA, 2008; GRR, 2018). This is similar to practice in the construction and demolition waste (CDW) industries, where crushing of concrete monoliths produces recycled concrete material (RCM; Sanger et al., 2020) for use in landscaping, void fill or as aggregate (Coudray et al., 2017; NDA, 2020). On-site reuse of RCM is an economically and environmentally advantageous route to minimizing both off-site waste transport and import of new materials for void fill and landscaping purposes (Deissmann et al., 2006; NDA, 2020).

In CDW industries, crusher fines are often removed from RCM prior to use as crushing can concentrate the alkaline cement paste in the finest fractions (Chen et al., 2019; Coudray et al., 2017; Engelsen et al., 2009). At nuclear sites, however, there is a desire to use RCM as backfill in much larger volumes than is common in the CDW industry, and to use it without fines removal to limit the need for off-site waste disposal (Foy et al., 2018). In addition, proposed uses of RCM at nuclear sites differ from more common RCM applications in that nuclear facilities often have deep basements that extend below the water table, and the RCM may be stockpiled for decades prior to use as it is mainly required at the end stages of decommissioning (NDA, 2020). RCM with a higher fines content would likely reduce the porosity and permeability of the backfill, leading to a decrease in water flow. However, the high surface area of the fines will increase the rate of cement phase dissolution, so there is uncertainty over whether fines inclusion will increase or decrease leaching. Further, RCM derived from the demolition of nuclear facilities will be subject to more stringent regulatory control due to the potential presence of low-level radioactivity, so there is a need to understand the leaching behavior of RCM over multi-decadal time scales to prepare the site closure safety cases.

---

* Corresponding author.
*E-mail address:* I.T.Burke@Leeds.ac.uk (I.T. Burke).

**Table 1**

Major element composition (wt%) of gravel, sand and fines fractions from surface 0 to 0.1 m (Surface) and sub-surface 2.5–2.7 m (Sub-S.) samples in trial pits RS1 and RS4 from stockpile 1 (SI Fig. S1 ), given as mean (n=6) $\pm 1\sigma$ of 6 replicates.

| | Major elemental composition (%) | | | | | | | | | |
| | Mg | Al | Si | P | S | K | Ca | Ti | Mn | Fe |
|---|---|---|---|---|---|---|---|---|---|---|
| **Gravel (6.3 – 20 mm)** | | | | | | | | | | |
| **Surface** | 0.6 ±0.2 | 1.2 ±0.4 | 24.2 ±1.1 | <0.1 | 0.2 ±0.1 | 0.3 ±0.0 | 9.5 ±0.8 | 0.3 ±0.2 | <0.1 | 1.3 ±0.3 |
| **Sub-S.** | 0.6 ±0.2 | 1.3 ±0.3 | 25.0 ±2.0 | <0.1 | 0.9 ±0.4 | 0.3 ±0.1 | 9.0 ±1.6 | 2.0. ±1.1 | 0.1 ±0.05 | 1.0 ±0.3 |
| **Sand (0.6 – 6.3 mm)** | | | | | | | | | | |
| **Surface** | 0.6 ±0.2 | 1.7 ±0.8 | 23.6 ±1.0 | <0.1 | 0.2 ±0.1 | 0.4 ±0.1 | 8.4 ±1.1 | 0.4 ±0.2 | <0.1 | 1.2 ±0.2 |
| **Sub-S.** | 0.6 ±0.2 | 1.6 ±0.5 | 24.2 ±1.5 | <0.1 | 0.6 ±0.4 | 0.4 ±0.1 | 8.3 ±1.4 | 1.6 ±1.1 | 0.1±0.05 | 1.0 ±0.2 |
| **Fines (< 0.6 mm)** | | | | | | | | | | |
| **Surface** | 0.6 ±0.2 | 2.2 ±0.5 | 23.3 ±1.8 | <0.1 | 0.2 ±0.1 | 0.5 ±0.1 | 7.7. ±1.4 | 0.5 ±0.1 | <0.1 | 1.3 ±0.2 |
| **Sub-S.** | 0.5 ±0.2 | 1.9 ±0.4 | 23.2 ±1.8 | <0.1 | 0.4 ±0.2 | 0.4 ±0.05 | 7.8 ±1.3 | 1.1 ±0.8 | 0.1 ±0.05 | 1.0 ±0.2 |

**Table 2**

Selected trace elements (ppm) concentrations in gravel (6.3–20 mm), sand (0.6–6.3 mm) and fines (<0.6 mm) sized fractions recovered from the surface (S) 0 – 0.1 m and sub-surface (D) 2.5–2.7 m in trial pits RS1 and RS4 from stockpile 1 (SI Fig S1), given as the mean (n=6) $\pm 1\sigma$ of 6 replicates..

| | Selected trace elements (ppm) | | | |
| | Cl | V | Cr | Pb |
|---|---|---|---|---|
| Gravel (6.3 – 20 mm) | | | | |
| Surface | <33 | 130 ±170 | 23 ±14 | 30 ±27 |
| Sub-S. | 260 ±46 | 1800 ±1100 | 110 ±50 | 120 ±89 |
| Sand (0.6 – 6.3 mm) | | | | |
| Surface | 140 | 183 ±155 | 31 ±15 | 44 ±26 |
| Sub-S. | 280 ±113 | 1400 ±1200 | 89 ±59 | 130 ±1 |
| Fines (< 0.6 mm) | | | | |
| Surface | 160 ±10 | 230 ±110 | 40 ±3 | 60 ±7 |
| Sub-S. | 210 ±33 | 830 ±840 | 67 ±44 | 140 ±130 |

Although fine and coarse aggregate (sand and gravel) dominate concrete composition by volume (Ekström, 2001), the hydrated cement paste is far more reactive and produces high pH when immersed in water (Deissmann et al., 2006). Hydrated cement paste is typically composed of non-stoichiometric hydrated calcium silicate gel (C-S-H, 40–45 %), portlandite (CH; 20–25%), monosulphate aluminate and trisulphate aluminate phases (respectively AFm; AFt; 10-20 %), minor hydroxides (e.g. KOH, NaOH; 0–5 %), and a pore solution (10–20 %) (Berner, 1992) (In this study, cement chemistry notation is used. Chemical composition of cement phases are detailed in SI Table S1). In Portland cement-based materials, C-S-H can readily incorporate aluminum, so is best regarded as a calcium aluminosilicate hydrate (C-(A)-S-H) with variable composition, which can be described in terms of the Ca/Si and Al/Si ratios, which is relevant for leaching (Gérard et al., 2002; L'Hôpital et al., 2016b, 2016a; L'Hôpital et al., 2015; Richardson, 1999).

The pore solution of fresh concrete contains $Na^+$, $K^+$, $OH^-$ and $Ca^{2+}$ ions due to dissolution of $Na_2O$ and $K_2O$ present in cement and equilibration with the hydrated cement phases, and usually has a pH value above 13 (Ekström, 2001; van der Sloot, 2000). When water with a pH lower than the pore solution comes into contact with cement phases, the very soluble Na- and K-hydroxides are leached out first, resulting in a decrease in the $OH^-$ concentration (Faucon et al., 1996). Leaching by pure water results in a cascade of cement dissolution processes that in turn control the pore water composition (the sequence of phases that control the solution chemistry are shown in SI Table S2). Initially, the decreasing pH value and leaching of calcium (decalcification) drives the dissolution of CH, then the other cement phases dissolve in sequence, with each in turn controlling the pore water composition (Ekström, 2001; Engelsen et al., 2009; Glasser et al., 2008). Carbonation also drives the decalcification of cement hydrates, as gaseous $CO_2$ dissolves into the pore solution, forming carbonate ions which react with $Ca^{2+}$ to form calcium carbonate (Glasser et al., 2008; Van Gerven et al., 2006). During carbonation and leaching, dissolution of the higher Ca/Si ratio cement hydrates occurs first producing cements with lower Ca/Si ratios over

time (Gérard et al., 2002; Segura et al., 2013). Highly alkaline leachate is produced at all stages of leaching, with the pore solution pH gradually decreasing from an initial pH of over 13 to around pH 9 over time (Jacques et al., 2014).

The successive changes in pore solution pH affects the stability of different cement phases and the leaching behaviour of any contaminants. Concrete can contain trace metal and other impurities, such as Ba, Cd, Co, Cr, Cu, Mn, Mo, Ni, Pb, Sb, Ti, V and Zn, which are derived from raw materials used for cement clinker production (Cornelis et al., 2008; Faucon et al., 1998; Vollpracht and Brameshuber, 2016). Oxyanion-forming contaminants (e.g. Co, Cr, Mo and V) are a particular concern, as they have enhanced solubility at the high pH values characteristic of concrete pore solutions (Gomes et al., 2016). RCM from nuclear sites may also contain radionuclides such as $^{137}$Cs, $^3$H, $^{60}$Co, $^{63}$Ni, U, Pu, Am and other actinide elements (Bath et al., 2003), however, this study specifically focused on alkalinity and stable element leaching from non-radioactive RCM produced during site decommissioning, which has been stockpiled for future use as void fill. Release of contaminants of potential concern from RCM is typically controlled by the dissolution of specific host cement phases, and their subsequent interactions (e.g. incorporation or sorption) with the secondary phases that form as the chemical conditions evolve during leaching (Engelsen et al., 2010; Vollpracht and Brameshuber, 2016).

This paper investigates the leaching behavior of non-radioactive crushed concrete that has been stockpiled at a nuclear licensed site undergoing decommissioning. The materials have been characterized, and pH-dependent batch leaching tests have been conducted on different size fractions from differently weathered samples from the same stockpile. These are used to determine the influence of size fraction, weathering after crushing and long-term stockpiling on the evolution of the leachate chemistry, and to evaluate the leaching behavior of selected elements (Ca, Si, Al, Mg, Fe, S, Pb, Cr, V, Cl) as function of pH. The data produced will inform safety assessments of in-situ disposal of crushed concrete as a void-filling material at UK nuclear sites.

## 2. Methods and Materials

### 2.1. Source of the crushed concrete

Crushed concrete from the demolition of various buildings across a UK nuclear licensed site was produced between 1997 and 2012. Subsequently this was stockpiled on site with the intention to use it as backfill in future site restoration activities. Characterization work carried out by the site managers involved the mechanical excavation of twenty-one trial pits at nineteen different locations at across the rubble stockpile, of which material from two trial pits (RS1 and RS4) where made available for this study (SI Fig. S1). Four samples outside the scope of UK nuclear regulations (total activity < 0.4 Bq g$^{-1}$; ~25 kg each) were obtained from the surface (0–0.1 m) and sub-surface (2.5–2.7 m) of each trial pit. Preliminary on-site processing involved spreading of the samples on benches and removal of foreign object debris such as metals, wood and electrical cable; leaving only cementitious and soil waste materials. Although there were variations between samples recovered from different trial pits, particle size analysis (in accordance with BS EN 933-1:2012; SI Fig. S2) indicated that on average particles >20 mm accounted for ~50% of the total sample mass, which were not further characterised in this study as they represent only a small fraction of the available surface area. The proportions of the stockpiled material in the smaller sizes were, ~25% between 6.3 and 20 mm, ~20% between 0.6 – 6.3 mm and ~5% < 0.6 mm (size fractionation is described below), and these size fractions were chosen for study.

### 2.2. Preparation of crushed concrete samples

For each of the four samples of crushed concrete obtained, 1.5–2 kg sub-samples were randomly taken from the bulk (~25 kg) sample to be used for laboratory experiments and dried at 40 °C overnight to remove moisture prior to fractionating using test sieves of 20 mm, 6.3 mm and 0.6 mm.

The size fractions chosen are based on ISO 14688-1:2017 (ISO 2017) which assigns:

6.3–20 mm: medium gravel (Gravel).
0.63–6.3 mm: fine gravel and coarse sand (Sand).
< 0.63 mm: medium and fine sand (Fines).

These size-fractions were then dried again at 40 °C overnight, and double-bagged in polyethylene self-seal bags, and stored in 2 L airtight glass jars.

### 2.3. Sample characterization

Each size fraction was placed on a clean polyethylene tray and homogenized before a portion was selected by coning and quartering for mineralogical and elemental characterization. Samples for mineralogical and chemical analysis were crushed first using a steel pestle and mortar followed by an Agate Tema barrel mill to <120 μm. Mineralogical analysis was undertaken using a Bruker D8 X-ray diffractometer (XRD), with the powder samples placed on silicon slides and scanned between 2 and 70 2$\theta$ using Cu K-alpha radiation. Major and selected trace elements (Cl, V, Cr and Pb) composition of the analytical samples were determined by X-ray Fluorescence (XRF) spectroscopy using Olympus Innovex X-5000.

Portions from the sand size-fraction from the surface and sub-surface samples were subjected to scanning electron microscopy-energy dispersive X-ray spectroscopy (SEM-EDS) analysis. Each SEM sample was set in epoxy resin (Huntsman Advanced Materials) and the surfaces of the resin blocks were polished using 3-, 1- and $\frac{1}{4}$-μm diamond paste (Struers) to expose cross-sections through the concrete grains. Back-scatter electron micrographs were obtain using a Tescan VEGA3 XM equipped with an Oxford instruments X-max 150 SDD EDS using Aztec 3.3 software. A beam energy of 15 keV was used, at a 15 mm working distance. Elemental mapping was performed at a resolution of 2 μm.

Point counting analysis was undertaken on false-colour composite EDS images of 5 representative particles from the surface and sub-surface samples (details in SI Section B; Fig. S3). EDS spot analysis was performed on 5 different particles in the surface and sub-surface samples by randomly selecting between 10 and 20 spots per particle. Maximum counts per second were set at 600,000 and calibration against a cobalt standard was performed regularly.

### 2.4. pH-dependent batch leaching experiments

Batch experiments were carried out on each of the three size fractions of the surface and sub-surface materials. The pH of the material at equilibrium was determined using deionized water without acid or base addition and is referred to as the material pH. Preliminary acid neutralization experiments were carried out to determine the approximate volume and strength of nitric acid (1–10 mol L$^{-1}$) or sodium hydroxide (1–5 mol L$^{-1}$) required to reach specific target pH values (between pH 2 and pH 13) for the batch experiments. Triplicate samples (4 g) were mixed with 40 ml deionized water (18 MΩ, *Millipore X500XX*) in 50 ml polyethylene tubes, and the pre-determined volumes of acid (HNO$_3$) or base (NaOH) were added to each suspension. Samples were agitated on an orbital shaker (70 ± 2 RPM), and further acid/base additions were made as required following measurement of the solution pH (suspensions were allowed to settle for 10 min prior to measurement). In some cases, several pH adjustments were required, and the experiments were run for either 7 or 8 days (the samples were equilibrated for at least a day after the last pH correction).

### 2.5. Analytical methods

Solution pH was measured using a Thermo Fisher Sure-Flow Electrode and Orion 3 Star pH meter, which was calibrated daily using pH buffers 4, 7, 10 and 12.46. At the end of testing, 10 mL of solution was taken from all replicates and filtered using a 0.22 μm polyethersulfone syringe filters. 1 mL of filtered solution was acidified with 2% HNO$_3$ (9 mL) for analysis of elements Ca, Si, Al, Mg, Fe, and S using a Thermo iCAP 7400 radial ion-coupled plasma optical emission spectrometer and Pb, Cr, and V using a Thermo iCAP Qc ion-coupled plasma mass spectrometer (ICP-MS), and the remainder of the filtered sample was stored without acid addition for anion analysis (Cl$^-$) by ion chromatography on a Thermo Scientific ICS5000. Samples were kept refrigerated at 4 °C before analysis.

## 3. Results

### 3.1. Characterisation of crushed concrete

The x-ray diffractograms from the sand and fine fractions (Fig. 1) have multiple large peaks at 2$\theta$ values characteristic of quartz, multiple clear peaks at 2$\theta$ values characteristic of calcite, and small peaks at 2$\theta$ values characteristic of dolomite, barite, muscovite and microcline. The identification of quartz and calcite as the major minerals present in both surface and sub-surface samples is supported by the major element XRF analysis (Table 1), where Si and Ca were the most abundant elements detected in all fractions, followed by Al, Fe, Ti, Mg, S, K, Mn and P. There were only minor compositional differences between the size fractions and between the surface and sub-surface samples although Ti was higher in the sub-surface fractions.

Trace element concentrations (Cl, V, Cr, Pb) were greater in the sub-surface fractions than in the surface fractions but were generally comparable across the size fractions of the same samples (Table 2). V concentrations were the highest out of all the trace elements measured (and also exhibited the most scatter), followed by Cl, Pb and Cr.

SEM-EDS analysis identified several distinct phases within the RCM particles. Phases dominated by either Si and O, or Ca and O, were consistent with the quartz and calcite phases detected by XRD. The most com-
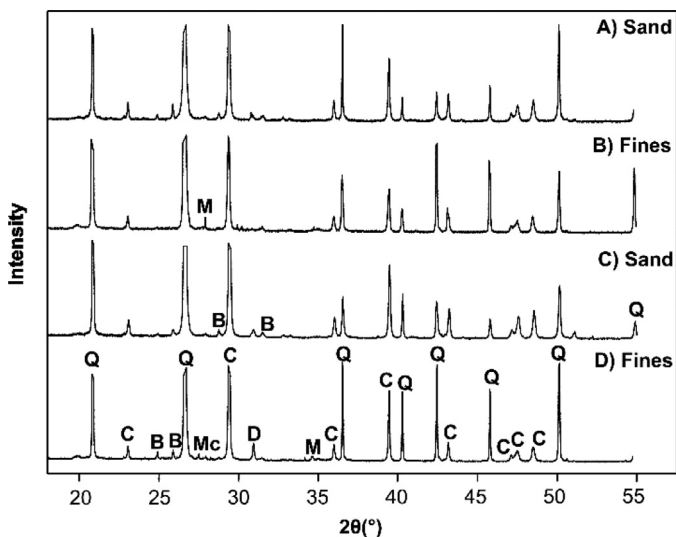
**Fig. 1.** Selected XRD patterns of sand (0.6–6.3 mm) and fines (< 0.6 mm) fractions of crushed concrete materials; A) and B) are from sub-surface (2.5–2.7 m) and C) and D) are from the surface 0–10 cm of trial pit RS4 from stockpile 1. Labelled minerals detected are quartz (Q), calcite (C), dolomite (D), barite (B), microcline (Mc) and muscovite (M). The major quartz and calcite peaks have been truncated to allow minor peaks from other phases to be discernible.

the surface and sub-surface samples show that quartz and calcite are often encased within a matrix material (containing Ca, Si and O with minor amounts of Al, S, Mg and Fe) with poorly defined margins and a variable Ca/Si composition, with local sub-regions that are Al-, S- or Ti-rich in the sub-surface samples, and Al-, Mg-, Fe- or S- rich in the surface samples. Point counting analysis, averaged across 5 false color SEM-EDS images, revealed that by volume the surface particles contained 22 $\pm$3 % quartz, 30 $\pm$3% calcite and 49 $\pm$4% matrix material, whilst sub-surface particles contained 18 $\pm$3% quartz, 12 $\pm$3% calcite and 70 $\pm$4% matrix material. Calcite is commonly present as thick surface coatings on the surface sample particles, which are thinner or absent on the sub-surface sample particles.

Both surface and sub-surface particles are predominantly composed of a Ca- and Si-rich matrix that differs in composition between the surface and sub-surface samples. The Ca/Si ratio of the matrix phase (derived from SEM-EDS spot analyses, Fig. 3) was 0.92 $\pm$ 0.28 in the sub-surface samples and 0.52 $\pm$ 0.32 in the surface samples. In the sub-surface samples, the majority of analyses where clustered close to that of an idealized C-(A)-S-H phase (Rossen and Scrivener, 2017) indicating that the predominant matrix phase is likely to be a mixture of amorphous C-(A)-S-H gel phases, which although abundant, are not detected by XRD. Other cement phases such as Aft and Hc/Mc (Fig. 3b) were also identified, and some compositions close to the C-S-H phase jennite were also observed. The SEM-EDS analyses of the surface material have a much greater spread in values and appear to spread away from the Al/Ca and Si/Ca ratios expected for C-(A)-S-H phases and towards progressively more Ca-depleted Si- and Al-rich phases.

### 3.2. Material pH and acid neutralization behavior

After suspension in deionized water for 7 days the aqueous pH was between 10 and 11.3 for the sub-surface material and between 8 and

mon particles seem in SEM micrographs were individual quartz grains, followed by particles consisting of a mixture of quartz and calcite particles within a matrix material that was dominated by Ca, Si and O but with sub-regions of varying chemical composition. The BSE and EDS maps (Fig. 2) collected from representative composite particles from
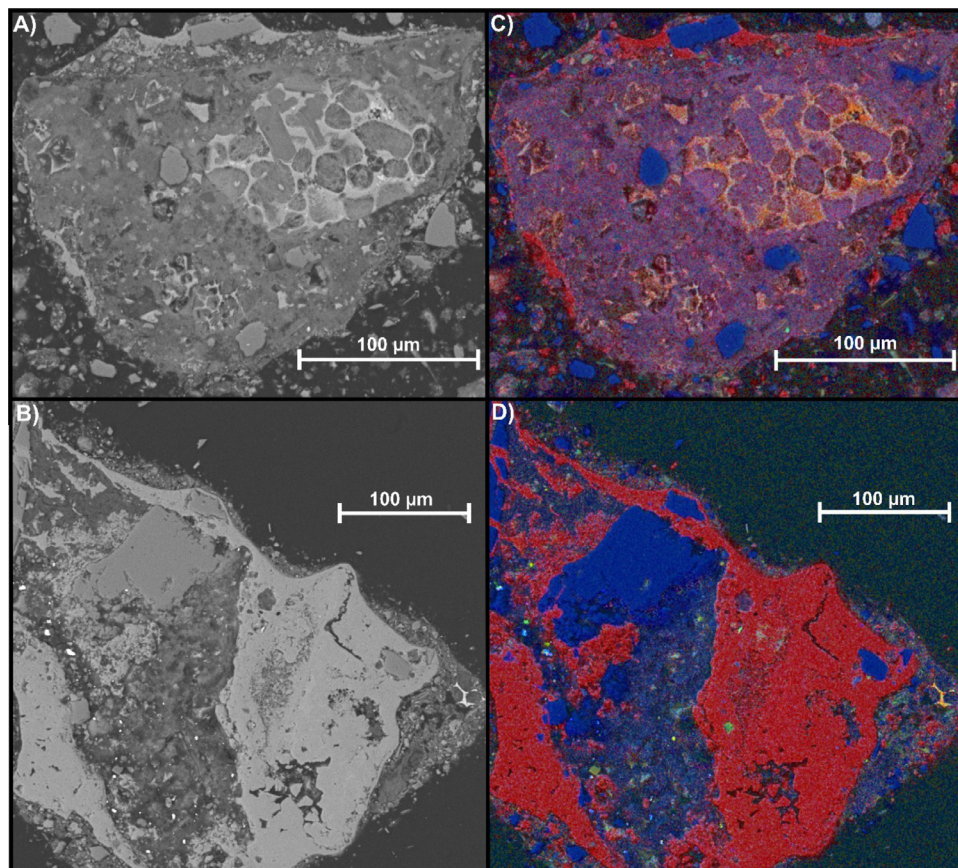


**Fig. 2.** SEM BSE images of sand-sized fraction (0.6–6.3 mm) of crushed concrete particles collected from trial pit RS4 from the A) sub-surface 2.5–2.7 below surface and B) surface 0–0.1 m of stockpile 1. C) and D) show corresponding sub-surface and surface false colour SEM-EDS elemental maps collected from the same locations where; Blue = Si, Red = Ca, Green = Fe, Orange = Mg, Yellow = S, Gold = Al, Magenta = Na (sub-surface only).
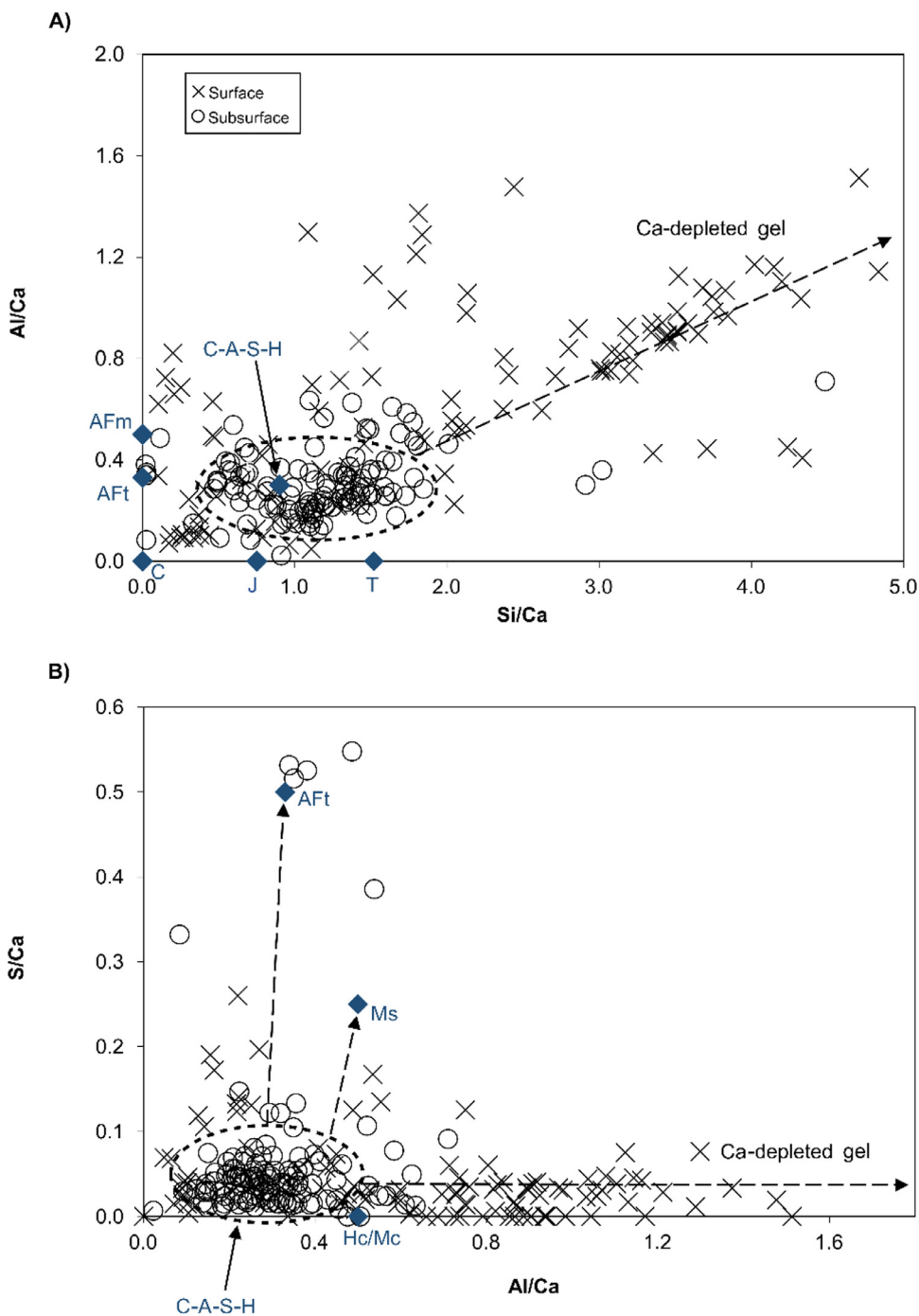
**Fig. 3.** Elemental ratios determined by SEM-EDS spot analysis of the matrix phase of sand-sized (0.6–6.3 mm) particles recovered from the surface (0 – 0.1 m) and sub-surface (2.5–2.7 m) layers of trial pit RS4 in stockpile 1. A) Elemental ratios Si/Ca against Al/Ca, and B) elemental ratios Al/Ca against S/Ca. Also plotted are the elemental ratios of selected phases from Rossen and Scrivener. (2017) including; calcium aluminate silicate hydrate (C-(A)-S-H), calcite (C), jennite (J) tobermorite (T), calcium aluminate monosulphate (AFm), calcium monosulphate (Ms), calcium hemi-carbonate/mono-carbonate (Hc/Mc), and calcium aluminate trisulphate (AFt). Oval represents the average matrix composition of the sub-surface samples ± 1σ; dotted arrows represent potential mixing lines between selected phases.

9.6 for the surface material, with a slight increase in pH observed with increasing size-fraction (Table 3). This pH value is hereafter denoted as the material pH and is equivalent to the short-term (1 week) equilibrium pH for these materials. The acid neutralization capacity (ANC) was similar in both sub-surface (Fig. 4a) and surface (Fig. 4b) samples and was greatest for the sand and fines fractions. Approximately 0.1–0.7 mmol $g^{-1}$ of acid was required to produce pH 7 (± 0.3) in experiments using both the sub-surface (Fig. 4a) and surface samples (Fig. 4b) with the sands and fines fractions falling at the upper end of the range. Larger differences between the size fractions were apparent in the volume of acid needed to reach pH 4 (± 0.3) with 3 and 4.8 mmol $g^{-1}$ required for the sand and fines fraction, whilst the gravel fraction required 1.4–2.6 mmol $g^{-1}$. In contrast, there was no discernible difference in base buffering capacity between the sub-surface and surface samples for any of the

size fractions tested, with only 0.3 mmol/g of NaOH required to raise pH >12 in both materials, indicating a low base buffering capacity.

### 3.3. Major element leaching as function of pH

At the material pH, the major elements leached from the sub-surface (Fig. 5; Table 4) and surface (SI Fig. S4) samples were (in order of concentration) Ca, Si, S, Al, Fe and Mg. Leaching behavior was similar for both sub-surface and surface samples. This similarity was also apparent as pH was altered outside the material pH range with the exception that Ca leaching from the sub-surface fractions was an order of magnitude higher than from the surface fractions over the pH range 8-9 (the unadjusted pH of the surface fraction).

**Table 3**
Mean and range of pH values of water in contact with gravel, sand and fines sized fractions of crushed concreate materials recovered from surface (0–0.1 m) and sub-surface (2.5–2.7 m) layer from trial pits RS1 and RS4 in stockpile 1 after suspension in deionised water for 7 days.

| Size fraction | Surface | Sub-surface |
| --- | --- | --- |
| Gravel (6.3–20 mm) | 9.1 (8.7–9.6) | 10.6 (10.0–11.3) |
| Sand (0.6–6.3 mm) | 8.7 (8.4–9.0) | 10.4 (10.2–10.7) |
| Fines (< 0.6 mm) | 8.3 (8.0–8.5) | 10.2 (9.9–10.5) |
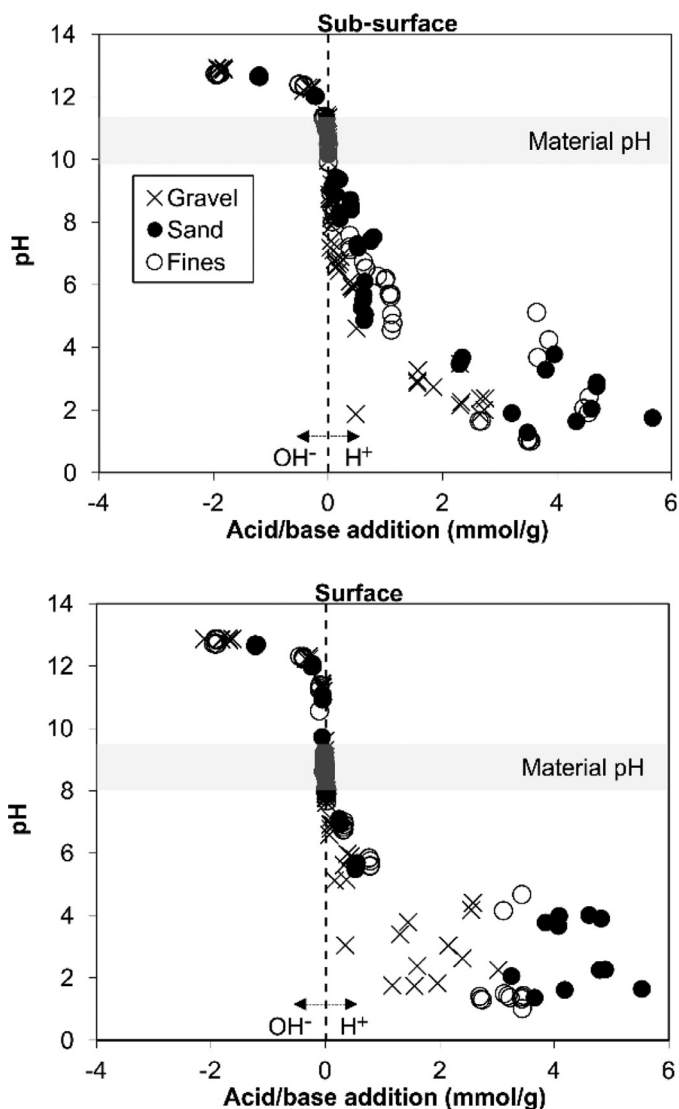


**Fig. 4.** Acid neutralising capacity of different crushed concrete size fractions recovered from the sub-surface (2.5–2.7 m) and surface( 0–0.1 m) layers of trial pits RS1 and RS4 from stockpile 1. Data from gravel (6.3–20 mm), sand (0.6–6.3 mm) and fines (< 0.6 mm) sized fractions are shown.

As pH was increased above the material pH range, Ca leaching progressively declined, Mg and Fe leaching remained at a minimum, and S release remained fairly constant for all size fractions (although there is scatter in the S concentration from both gravel fractions). The leaching of Si and Al increased as pH was raised above the material pH. When pH was lowered below the material pH, leaching of Ca and Mg increased by several orders of magnitude as pH became increasingly acidic. Leaching of Fe was not observed until pH was <5, while S release increased grad-

**Table 4**
Mean and range of aqueous elemental concentrations for all size fractions from surface (0 – 0.1 m) and sub-surface (2.5–2.7 m) samples of trial pits RS1 and RS4 from stockpile 1 in leaching experiments after 7 days equilibrium with deionised water.

| Determinand | Units | Surface | Sub-surface |
| --- | --- | --- | --- |
| pH | - | 8.7 (8.0–9.6) | 10.4 (9.9–11.3) |
| Ca | (mg L$^{-1}$) | 3.7 (1.7–5.4) | 5.9 (2.6–10.2) |
| Si | (mg L$^{-1}$) | 1.2 (0.3–2.7) | 2.1 (1.1–3.6) |
| Fe | (mg L$^{-1}$) | 0.1 (0.1–0.1) | 0.1 (0.1–0.1) |
| Al | (mg L$^{-1}$) | 0.3 (0.2–0.5) | 0.3 (0.1–0.4) |
| Mg | (mg L$^{-1}$) | 0.1 (0.1–0.1) | 0.1 (0.1–0.1) |
| S | (mg L$^{-1}$) | 1.1 (0.2–3.1) | 1.9 (0.5–4.1) |
| Cl$^-$ | (mg L$^{-1}$) | 6.1 (2.9–19.7) | 4.8 (2.1–8.1) |
| Pb | ($\mu$g L$^{-1}$) | 0.2 (0.2–0.4) | 0.2 (0.1–0.4) |
| Cr | ($\mu$g L$^{-1}$) | 1.0 (0.4–2.6) | 2.2 (0.4–12.9) |
| V | ($\mu$g L$^{-1}$) | 1.3 (0.3–4.4) | 2.1 (0.6–3.8) |

ually as pH was lowered. All elements measured reached the greatest concentrations at pH ≤ 2. Although there is greater sample variability in the behavior of the gravel-sized material (especially for S), there appears to be no systematic differences in the leaching behavior between the size fractions of either the sub-surface or surface materials.

### 3.4. The pH-dependent release of Pb, Cr, V and Cl$^-$

At the material pH values, the trace element leaching concentrations were similar in the size fractions of both sub-surface (Fig. 6) and surface (SI Fig. S5) samples, despite the sub-surface samples having higher trace element concentrations in the solid (Table 1). When the pH was adjusted outside the material pH range, there were generally only modest differences in the leaching of trace metals between the sub-surface and surface samples and between the different size fractions, although scatter is apparent for Cr, V and Cl$^-$ release from the gravel fraction.

For all fractions, Pb leaching was at a minimum between pH 6-11 and typically rose by several orders of magnitude as pH was adjusted above and below this range, with greatest release at pH ≤ 4. Between pH 6 and pH >12, Cr release was relatively constant (except for gravel samples), whilst V release was similarly constant between pH 6-9, and gradually increased as pH rose. Between pH 4 and 5, V and Cr release was at a minimum, but as pH was lowered below <4, leaching progressively rose by two orders of magnitude. In contrast, Cl$^-$ showed no pH-dependent leaching pattern and generally remained relatively consistent across all pH values.

## 4. Discussion

### 4.1. Composition and characterisation of crushed concrete

The crushed concrete material sourced from the sub-surface (2.5–2.7 m) and the surface (0–0.1 m) of the stockpile at this site was found to consist primarily of silica grains (quartz sand) and calcite in a C-(A)-S-H matrix, containing some phases close in composition to pure phase Hc/Mc, AFm and jennite (Fig. 3). Evidence of weathering is apparent in both sub-surface and surface samples; no portlandite (CH) was detected in X-ray diffraction patterns (Fig. 1), which indicates that both samples have been leached by rainwater during storage, removing more soluble cement phases. Calcite is a common product of cement carbonation involving reaction with atmospheric $CO_2$ (Chen et al., 2013; Šavija and Luković, 2016). Although both materials contain carbonate phases (calcite, dolomite), the particles in the surface samples have a more distinct calcium carbonate layer and greater proportion of calcite measured by point counting (Fig. 2; Section 3.1).

The material pH values for the sub-surface (pH 10–11.3) and surface (pH 8–9.6) samples are consistent with that of hardened cement paste that has undergone weathering and carbonation (i.e. pH is below the
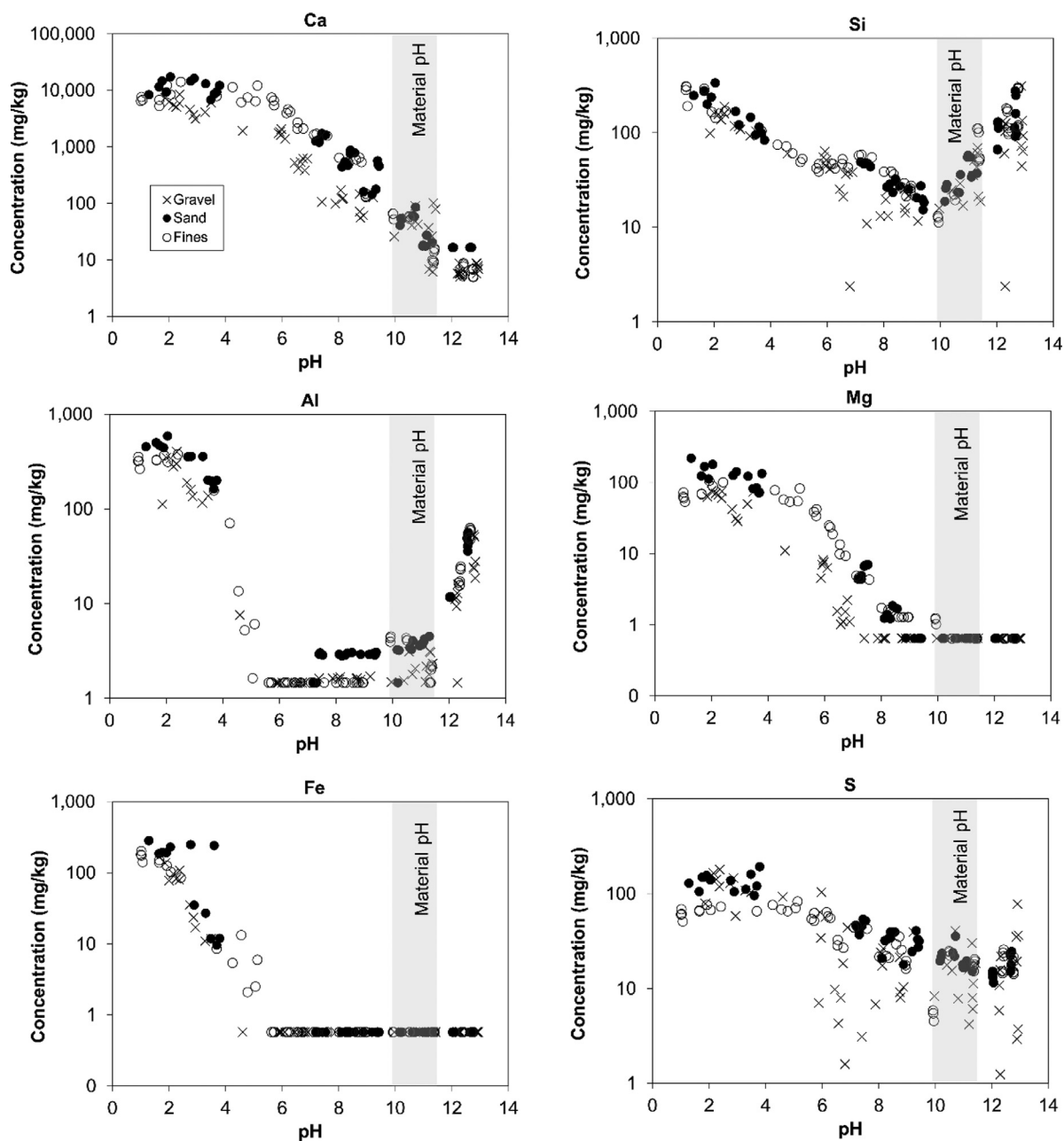
**Fig. 5.** Leaching of major elements Ca, Si, Al, Mg, Fe and S from the sub-surface (2.3–2.7 m) crushed concrete gravel, sand and fines sized fractions from trial pit RS1 and RS4 of stockpile 1 as a function of pH. Material pH denotes the range of aqueous pH values measured after suspension in deionised water for 7 days.

portlandite equilibrium pH of 12.4; Table 3) (Garrabrants et al., 2004). As carbonation results in the progressive neutralization of the pore solution to < pH 9 (Garrabrants et al., 2004), the lower material pH of the surface samples are evidence of a greater degree of both weathering and carbonation relative to the sub-surface samples. Indeed, the lower material pH values of the surface material are consistent with leaching of calcium carbonate phases (e.g. at log $PCO_2$ = -3.5 the equilibrium pH of calcite in water is 8.3; (Langmuir, 1997)), whilst the higher material pH values found for the subsurface materials are attributed to leaching of the C-(A)-S-H gel. The substantially lower Ca/Si ratio of the C-(A)-S-H gel in surface particles (Ca/Si = 0.52 ± 0.32) relative to sub-surface particles (Ca/Si = 0.92 ± 0.28) provides further evidence of extensive decalcification that has occurred in the surface samples, and is consistent with the lower surface material pH values (Glasser et al., 2008; Lagerblad, 2001; Šavija and Luković, 2016). Leaching of the surface ma-

terial may for a time, therefore, be controlled by carbonate dissolution, although the material at the stockpile surface only represents a minor portion of concrete rubble for disposal.

The C-(A)-S-H phases in a hardened cement paste is typically a C-S-H matrix with some alumina bonding between the Si chains and sheets (i.e. a mixed C-(A)-S-H / C-S-H phase), therefore the leaching behavior of C-(A)-S-H can be compared directly to that of C-S-H. The material pH and Ca/Si ratio of C-(A)-S-H in the sub-surface samples are consistent with leaching of C-S-H phases with Ca/Si ratios of 0.85–1.0, which dissolve incongruently and commonly buffers cement waters to pH values between 10 and 11 (Atkinson, 1985; Walker et al., 2016). Higher Ca/Si ratio C-S-H phases are shown to preferentially leach Ca into solution relative to Si (Harris et al., 2002), and are associated with higher pH values, so it is likely that the leaching of the sub-surface material during in-situ disposal will initially reflect the relatively high Ca/Si ratio C-(A)-S-H
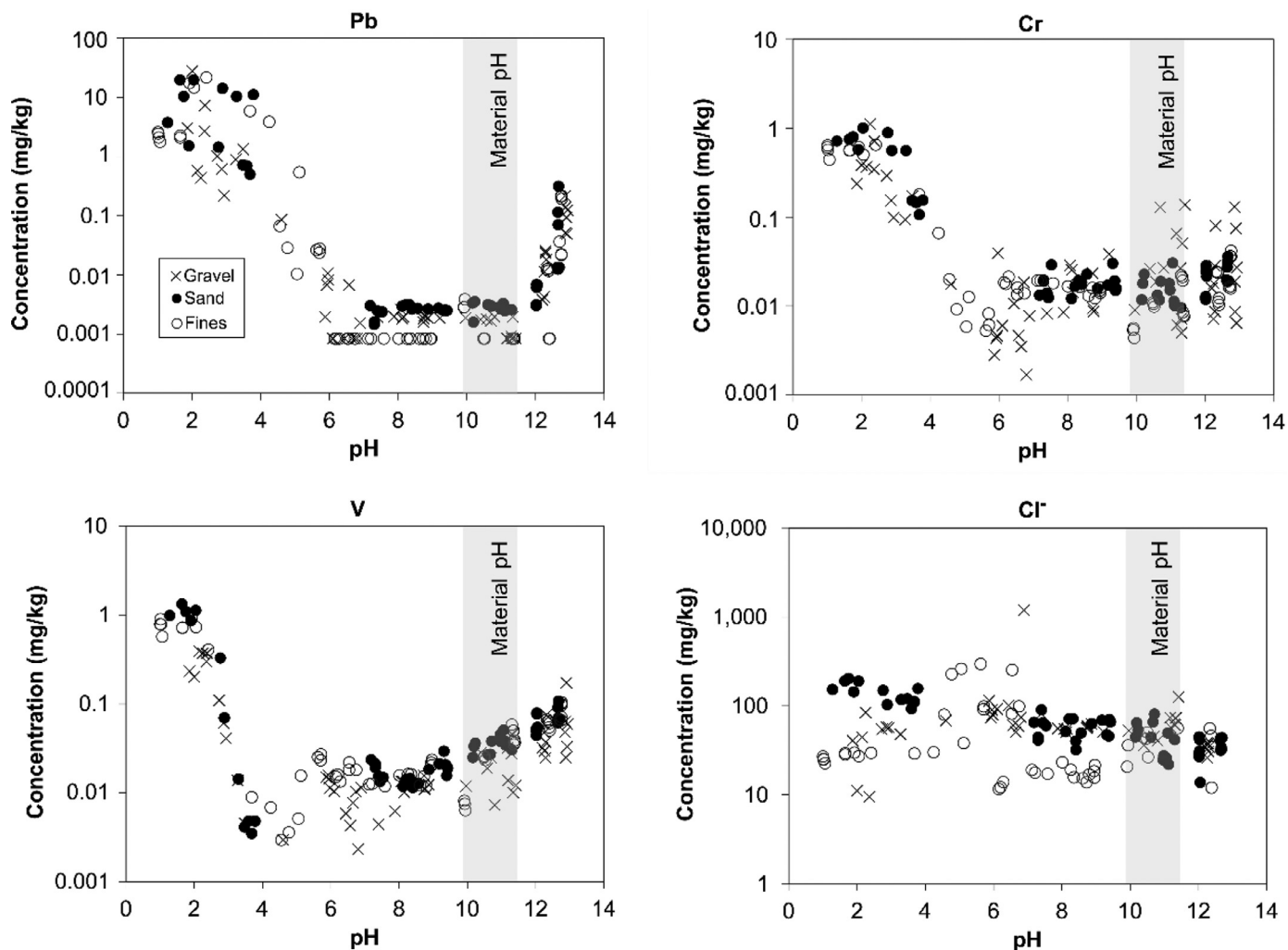
**Fig. 6.** Leaching of Pb, Cr, V and Cl⁻ from the sub-surface (2.3–2.7 m) crushed concrete gravel, sand and fines sized fractions from trial pit RS1 and RS4 in stockpile 1 as a function of pH. Material pH denotes the range of aqueous pH values measured after suspension in deionised water for 7 days.

phases, until they are exhausted, producing an equilibrium pH between 10 and 11. This reaffirms that partially carbonated RCM can still produce a high pH eluate in leaching tests (Engelsen et al., 2009; Foy et al., 2018; Mahedi and Cetin, 2020).

*4.2. Chemical stability and leaching of crushed concrete*

If crushed concrete wastes are ultimately used as site infill within existing below ground structures, the material may become in contact with water from surface infiltration and groundwater ingress. The equilibrium test results are therefore beneficial for understanding how the RCM could behave when saturated with water.

In terms of size fraction, the consensus in the nuclear (and CDW) sector is to avoid the use of fines from freshly crushed concrete, due to the potential production of high pH leachates (Foy et al., 2018). Although this generally applies for fines from freshly crushed concrete (as uncarbonated surfaces are exposed), this is not observed in the present study; long-term (10 to >20 years) stockpiling of crushed concrete has resulted in lower material pH for the fines fraction relative to larger size fractions (Table 3). This trend of pH reducing with size fraction of RCM was also observed by Chen et al (2012) who used similar size fractions (gravel 4.75 -75 mm, sand 0.075–4.75 mm and fines, <0.075 mm) and was attributed to a higher degree of carbonation during storage due to an increased reactive surface area in smaller particles. There are also concerns with the potential for enhanced leaching from fines, due

to increased surface area. Although crushed concrete fines have higher surface area relative to larger particles, which theoretically would increase leaching, no substantial differences were observed in this study. Similarities in leachate composition between the size fractions after 1 week suggests that leaching was independent of surface area and may be under equilibrium control. This indicates an overall beneficial impact of long-term stockpiling after crushing RCM before eventual on-site use as fill. The lower material pH of the fines implies no need for their deliberate removal and if desired the fines for stockpiled RCM could even be suitable for re-use as fine aggregate in cement grouts (Foy et al., 2018).

An approximate calculation of the volume of alkaline leachate that will be generated by onsite disposal of CDW can be made using the ANC test results. If rainwater or acidic groundwater with a pH value of 5 ([H⁺] = 1 x 10⁻⁵ mol L-1) were to infiltrate RCM backfill material, it would require approximately 10-70 x 10³ L of water per kg of the backfill material to lower the pH to 7. However, surface infiltration is expected to be minimal at nuclear sites due to use of engineered caps with low permeability and the rate of groundwater ingress through existing concrete structures (wall and floors) is also expected to be low. It is therefore, more likely that the pore waters within the disposal volume will equilibrate with the RCM producing aqueous compositions similar to batch leaching tests using the sub-surface materials (Table 4). This composition can be expected to be stable over long time scales (provided that groundwater flow rates remain low). Egress of water from the disposal structure will also be low and may produce a small alka-

line plume downstream of the structure, the scale of which will depend on the alkaline buffering capacity of the surrounding soils. However, if the RCM is used for landscaping purposes in unlined structures, then leachate will be released more readily into the surrounding soils. If local soil waters are acidic in nature, unacceptable leaching of contaminant metals such as Al, Cr, Pb and V that are much more mobile at low pH (Figs. 5 and 6) may also occur. Therefore, the use of RCM as fill in situations where contact with low pH soil waters is expected is not advised.

### 4.3. Implications for management of void-filling

The priority for management of void-filling is to reduce the potential for the generation and egress of alkaline leachate and associated contaminant metals or radionuclides. While some water ingress is inevitable, reducing the volume of groundwater ingress through the grouting of internal voids is a potential solution. Grouting reduces the pore volume and particularly surface area of material in contact with any pore water, restricting contact with RCM to cracks in the grout. However, the use of a conventional ordinary Portland cement grout should be avoided, as the high pH of fresh cement pore water (pH > 13) could be problematic as the RCM has a low base buffering capacity, therefore, metals that are mobile at high pH such as Al, V and Pb could be released into solution.

It is recommended that the appropriate chemical composition is assumed for the RCM when modelling in-situ disposal as part of any site-specific risk assessment. Otherwise, the modelling results will be overly conservative, as freshly crushed concrete typically contains portlandite which can generate leachate with pH values >12, whereas the stockpiled RCM material analyzed in this study was devoid of portlandite and the subsequent leaching behavior was dominated by C-(A)-S-H phases. However, it will be important to account for any weathering of RCM after it has been crushed. The Ca/Si ratio of the C-(A)-S-H phases in the RCM varied with post-crushing weathering, with more weathered material dominated by C-(A)-S-H phases with a lower Ca/Si ratio, and abundant calcite from carbonation, producing a more benign leachate. Thus, it may be appropriate in a conservative model to assume that leaching is dominated by C-(A)-S-H with a Ca/Si ratio between 0.8 and 1.0 and a tobermorite-like structure, unless extensive weathering and carbonation has been confirmed.

## 5. Conclusion

The crushed concrete samples from the sub-surface (2.5–2.7 m) and surface (0–0.1 m) locations consisted mainly of silica and calcite grains encased in a C-(A)-S-H matrix of varying composition. Calcite, which was more abundant in the surface samples, was present mainly on particle surfaces and resulted from carbonation of cement phases during weathering. More highly weathered surface materials contained C-(A)-S-H gel phases with a Ca/Si ratio of $52 \pm 0.32$ and produced less alkaline leachate in leaching tests (pH 8–9.6). Whereas less weathered subsurface materials contained C-(A)-S-H gel phases with a Ca/Si ratio of $0.92 \pm 0.28$ and produced a more alkaline leachate (pH 10–11.3). Dissolution of major elements, such as Ca and Si, and leaching of trace contaminants, such as Al, Pb, Cr and V, was generally minimized in the pH range produced by equilibrium with either surface or sub-surface samples but increased by several orders of magnitude as pH was either raised above pH 12 or lowered below pH 5. Despite the pH-difference, the two materials produced leachate with similarly benign elemental compositions from all size fractions, suggesting that fines removal is not required prior to the use of stockpiled RCM as a fill material.

### Declaration of Competing Interests

The authors declare that they have no known competing financial interests or personal relationships that could have appeared to influence the work reported in this paper.

### Supplementary materials

Supplementary material associated with this article can be found, in the online version, at doi:10.1016/j.hazadv.2021.100043.

## References

Atkinson, A., 1985. The time dependence of pH within a repository for radioactive waste disposal. UKAEA Atomic Energy Research Establishment. AERE R11777. HMSO, London, UK.

Bath, A., Deissmann, G., Jefferis, S., 2003. Radioactive contamination of concrete: uptake and release of radionuclides. In: International Conference on Radioactive Waste Management and Environmental Remediation, 37327, pp. 1155–1162.

Berner, U.R., 1992. Evolution of pore water chemistry during degradation of cement in a radioactive waste repository environment. Waste Manag. 12, 201–219.

Chen, J., Sanger, M., Ritchey, R., Edil, T., Ginder-Vogel, M., 2019. Neutralization of high pH and alkalinity effluent from recycled concrete aggregate (RCA) by common subgrade soil. J. Environ. Qual. 49, 172–183.

Chen, J., Tinjum, J., Edil, T., 2013. Leaching of alkaline substances and heavy metals from recycled concrete aggregate used as unbound base course. Transp. Res. Rec.: J. Transp. Res. Board 2349, 81–90.

Cornelis, G., Johnson, C.A., Gerven, T.V., Vandecasteele, C., 2008. Leaching mechanisms of oxyanionic metalloid and metal species in alkaline solid wastes: a review. Appl. Geochem. 23, 955–976.

Coudray, C., Amant, V., Cantegrit, L., Le Bocq, A., Thery, F., Denot, A., Eisenlohr, L., 2017. Influence of crushing conditions on recycled concrete aggregates (RCA) leaching behaviour. Waste Biomass Valoriz. 8, 2867–2880.

Deissmann, G., Bath, A., Jefferis, S., Thierfeldt, S., Wörlen, S., 2006. Development and application of knowledge-based source-term models for radionuclide mobilisation from contaminated concrete. MRS Online Proc. Lib. 932, 1–8.

Ekström, T., 2001. Leaching of Concrete: Experiments And Modelling PhD Thesis. Lund University, Sweden.

Engelsen, C.J., van der Sloot, H.A., Wibetoe, G., Justnes, H., Lund, W., Stoltenberg-Hansson, E., 2010. Leaching characterisation and geochemical modelling of minor and trace elements released from recycled concrete aggregates. Cem. Concr. Res. 40, 1639–1649.

Engelsen, C.J., van der Sloot, H.A., Wibetoe, G., Petkovic, G., Stoltenberg-Hansson, E., Lund, W., 2009. Release of major elements from recycled concrete aggregates and geochemical modelling. Cem. Concrete Res. 39, 446–459.

Faucon, P., Adenot, F., Jacquinot, J.F., Petit, J.C., Cabrillac, R., Jorda, M., 1998. Long-term behaviour of cement pastes used for nuclear waste disposal: review of physico-chemical mechanisms of water degradation. Cem. Concr. Res. 28, 847–857.

Faucon, P., Le Bescop, P., Adenot, F., Bonville, P., Jacquinot, J.F., Pineau, F., Felix, B., 1996. Leaching of cement: study of the surface layer. Cem. Concr. Res. 26, 1707–1715.

Foy, J., Jones, G., Sephton, M., Gaitonde, R., 2018. Managing on-Site Stockpiling and use of High Volumes of Concrete-Based Demolition Material. Nuclear Decommissioning Authority, Cumbria, UK, pp. 1–49.

Garrabrants, A.C., Sanchez, F., Kosson, D.S., 2004. Changes in constituent equilibrium leaching and pore water characteristics of a Portland cement mortar as a result of carbonation. Waste Manag. 24, 19–36.

Gérard, B., Le Bellego, C., Bernard, O., 2002. Simplified modelling of calcium leaching of concrete in various environments. Mater. Struct. 35, 632–640.

Glasser, F.P., Marchand, J., Samson, E., 2008. Durability of concrete — degradation phenomena involving detrimental chemical reactions. Cem. Concr. Res. 38, 226–246.

Gomes, H.I., Mayes, W.M., Rogerson, M., Stewart, D.I., Burke, I.T., 2016. Alkaline residues and the environment: a review of impacts, management practices and opportunities. J. Clean. Prod. 112, 3571–3582.

, 2018. Management of Radioactive Waste from Decommissioning of Nuclear Sites. Scottish Environmental Agency, Environment. Agency and Natural Resources Wales (Eds.), p. 98.

Harris, A.W., Manning, M.C., Tearle, W.M., Tweed, C.J., 2002. Testing of models of the dissolution of cements—leaching of synthetic CSH gels. Cem. Concr. Res. 32, 731–746.

IAEA, 2008. Managing Low Radioactivity Material from the Decommissioning of Nuclear Facilities. International Atomic Energy Agency, Vienna, Austria Technical Report Series No. 462.

ISO, 2017. ISO 14688-1: 2017 Geotechnical Investigation And Testing — Identification and Classification of Soil — Part 1: Identification and Description. International Organization for Standardization, Geneva, Switzerland.

Jacques, D., Perko, J., Seetharam, S.C., Mallants, D., 2014. A cement degradation model for evaluating the evolution of retardation factors in radionuclide leaching models. Appl. Geochem. 49, 143–158.

Jefferson, P., 2009. *The risks of reclamation.* Professional Broking, 02 Sept 2009. URL: www.insuranceage.co.uk/professional-broking/analysis/1531918/the-risks-reclamation. (Last accessed 25th Oct 2021).

L'Hôpital, E., Lothenbach, B., Scrivener, K., Kulik, D.A., 2016. Alkali uptake in calcium alumina silicate hydrate (C-A-S-H). Cem. Concr. Res. 85, 122–136.

L'Hôpital, E., Lothenbach, B., Kulik, D.A., Scrivener, K., 2016. Influence of calcium to silica ratio on aluminium uptake in calcium silicate hydrate. Cem. Concr. Res. 85, 111–121.

L'Hôpital, E., Lothenbach, B., Le Saout, G., Kulik, D., Scrivener, K., 2015. Incorporation of aluminium in calcium-silicate-hydrates. Cem. Concr. Res. 75, 91–103.

Lagerblad, B., 2001. Leaching Performance of Concrete Based on Studies of Samples from Old Concrete Constructions. Leaching Performance of Concrete Based on Studies of Samples from Old Concrete Constructions, 1. Svensk Kärnbränslehantering AB, Stockholm, Sweden.

Langmuir, D., 1997. Aqueous Environmental Geochemistry. Prentice Hall, Upper Saddle River, N.J. USA.

Mahedi, M., Cetin, B., 2020. Carbonation based leaching assessment of recycled concrete aggregates. Chemosphere 250, 126307.

NDA, 2010. UK Strategy for the Management of Solid Low Level Radioactive Waste from the Nuclear Industry. Nuclear Decommissioning Authority, Cumbria, UK.

NDA, 2020. *Concrete example of dealing with decommissioning rubble*. Nuclear Decommissioning Authority. 06 Jan 2020. URL: https://www.gov.uk/government/case-studies/concrete-example-of-dealing-with-decommissioning-rubble. (Last accessed 24 Oct 2021).

Richardson, I.G., 1999. The nature of C-S-H in hardened cements. Cem. Concr. Res. 29, 1131–1147.

Rossen, J. E., Scrivener, K. L., 2017. Optimization of SEM-EDS to determine the C–A–S–H composition in matured cement paste samples. Materials Characterization 123, 294–306. doi:10.1016/j.matchar.2016.11.041.

Sanger, M., Natarajan, B.M., Wang, B., Edil, T., Ginder-Vogel, M., 2020. Recycled concrete aggregate in base course applications: review of field and laboratory investigations of leachate pH. J. Hazard. Mater. 385, 121562.

Šavija, B., Luković, M., 2016. Carbonation of cement paste: understanding, challenges, and opportunities. Constr. Build. Mater. 117, 285–301.

Segura, I., Molero, M., Aparicio, S., Anaya, J.J., Moragues, A., 2013. Decalcification of cement mortars: characterisation and modelling. Cem. Concr. Comp. 35, 136–150.

van der Sloot, H.A., 2000. Comparison of the characteristic leaching behavior of cements using standard (EN 196-1) cement mortar and an assessment of their long-term environmental behavior in construction products during service life and recycling. Cem. Concr. Res. 30, 1079–1096.

Van Gerven, T., Cornelis, G., Vandoren, E., Vandecasteele, C., Garrabrants, A.C., Sanchez, F., Kosson, D.S., 2006. Effects of progressive carbonation on heavy metal leaching from cement-bound waste. AIChE J. 52, 826–837.

Vollpracht, A., Brameshuber, W., 2016. Binding and leaching of trace elements in Portland cement pastes. Cem. Concr. Res. 79, 76–92.

Walker, C.S., Sutou, S., Oda, C., Mihara, M., Honda, A., 2016. Calcium silicate hydrate (C-S-H) gel solubility data and a discrete solid phase model at 25 ℃ based on two binary non-ideal solid solutions. Cem. Concr. Res. 79, 1–30.